Editors' Suggestion

Electron-phonon coupling and competing Kekulé orders in twisted bilayer graphene

Yves H. Kwan,[1] Glenn Wagner,[2] Nick Bultinck,[3,4] Steven H. Simon,[3] Erez Berg,[5] and S. A. Parameswaran[3]

[1]*Princeton Center for Theoretical Science, Princeton University, Princeton, New Jersey 08544, USA*
[2]*Department of Physics, University of Zurich, Winterthurerstrasse 190, 8057 Zurich, Switzerland*
[3]*Rudolf Peierls Centre for Theoretical Physics, Parks Road, Oxford, OX1 3PU, United Kingdom*
[4]*Department of Physics, Ghent University, Krijgslaan 281, 9000 Gent, Belgium*
[5]*Department of Condensed Matter Physics, Weizmann Institute of Science, Rehovot 76100, Israel*

(Received 11 May 2023; accepted 13 August 2024; published 29 August 2024)

Recent scanning tunneling microscopy experiments in twisted bilayer [K. P. Nuckolls *et al.*, Nature (London) **620**, 525 (2023)] and trilayer [H. Kim *et al.*, Nature (London) **623**, 942 (2023)] graphene have revealed the ubiquity of Kekulé charge-density wave order in magic-angle graphene. Most samples are moderately strained and show "incommensurate Kekulé spiral" (IKS) order involving a graphene-scale charge density distortion uniaxially modulated on the scale of the moiré superlattice, in accord with theoretical predictions. However, ultralow strain bilayer samples instead show graphene-scale Kekulé charge order that is uniform on the moiré scale. This order, especially prominent near filling factor $\nu = -2$, is unanticipated by theory which predicts a time-reversal breaking Kekulé current order at low strain. We show that including the coupling of moiré electrons to graphene-scale optical zone-corner (ZC) phonons stabilizes a uniform Kekulé charge ordered state at $|\nu| = 2$ with a quantized topological (spin or anomalous Hall) response. Our work clarifies how this phonon-driven selection of electronic order emerges in the strong-coupling regime of moiré graphene.

DOI: 10.1103/PhysRevB.110.085160

I. INTRODUCTION

The interplay of strong electron correlations, gate-tunable superconductivity, and band topology in "magic-angle" twisted bilayer graphene (MA-TBG) has been the subject of extensive experimental [1–36] and theoretical investigation [37–72]. Although aspects of the phenomenology superficially resemble that of the cuprate high-temperature (high-T_c) superconductors, the nontrivial topology of the eight bands straddling charge neutrality, and the existence of Stoner-like transitions indicative of the formation of flavor-polarized broken-symmetry states, challenge the applicability of the Hubbard-type models familiar from high-T_c to the narrow bands in MA-TBG. This has stimulated a distinct perspective [40,50] rooted instead in the physics of quantum Hall ferromagnets (QHFM), best motivated by the approximation of initially ignoring the single-particle dispersion and working in the "chiral limit" [73] of vanishing interlayer same-sublattice tunneling. In the resulting strong-coupling problem, flavor-polarized insulators minimize the interaction energy (owing to Pauli exclusion) at densities of $|\nu| = 0, 1, 2, 3$ electrons per moiré unit cell, corresponding to filling $\nu + 4$ of the eight central bands. Single-particle terms and realistic interlayer tunneling perturbatively lift the large degeneracy of the resulting manifold of broken-symmetry states, selecting specific correlated insulators at integer ν [40,45,50].

Strong-coupling approaches predict gapped insulators at charge neutrality ($\nu = 0$) and time-reversal breaking quantized anomalous Hall (QAH) behavior or stripe order at odd ν [46,75]. This is in contradiction to many experiments, that often find semimetallic behavior $\nu = 0$ [1–3,5–13], little transport evidence for gaps at $\nu = \pm 1$, and no QAH response at $\nu = \pm 3$ unless aligned with a hexagonal boron nitride substrate [14,15]. Spurred by this mismatch of theory and experiment, Ref. [54] proposed a new type of broken-symmetry order, dubbed the incommensurate Kekulé spiral (IKS), as the ground state for MA-TBG at intermediate coupling. For modest uniaxial heterostrains [32–35] (where layers are strained relative to each other) sufficient to stabilize a semimetal at neutrality [65], IKS is the unique Hartree-Fock ground state for all nonzero integer $|\nu| < 4$. It exhibits a clear gap and vanishing QAH response for $|\nu| = 2, 3$, and is gapless for $|\nu| = 1$, consistent with most transport experiments. IKS order also persists to finite doping away from integer ν, seeding Fermi surfaces [76] consistent with Landau fans observed in magnetotransport [1–9,14–18]. Most strikingly, IKS involves a specific graphene-scale Kekulé charge density order that triples the graphene unit cell but is slowly modulated on the moiré scale. This multiscale spatial symmetry-breaking is a sharp signature of IKS order, recently used to diagnose its presence via scanning tunneling microscopy (STM) in MA-TBG [19] and its closely related cousin mirror-symmetric twisted trilayer graphene (TTG) [77].

These experiments find robust IKS order in samples with modest strain, with a period of approximately three moiré unit cells, in excellent agreement with theoretical predictions. However, at $\nu = -2$ where the data are most extensive, ultralow-strain samples reported in Ref. [19] show Kekulé charge order that also triples the graphene unit cell, but is at $q = 0$, i.e., unmodulated on the moiré scale, in sharp contrast to IKS. This contradicts the near-unanimous theoretical prediction in this limit of a $q = 0$ Kekulé current order, dubbed the "Kramers-Intervalley Coherent" (KIVC) state, whose STM signature vanishes by symmetry [78,79]. Instead, the observed order resembles the so-called TIVC state ("T" denotes a spinless implementation of time reversal), which can be viewed roughly as a charge counterpart of KIVC.

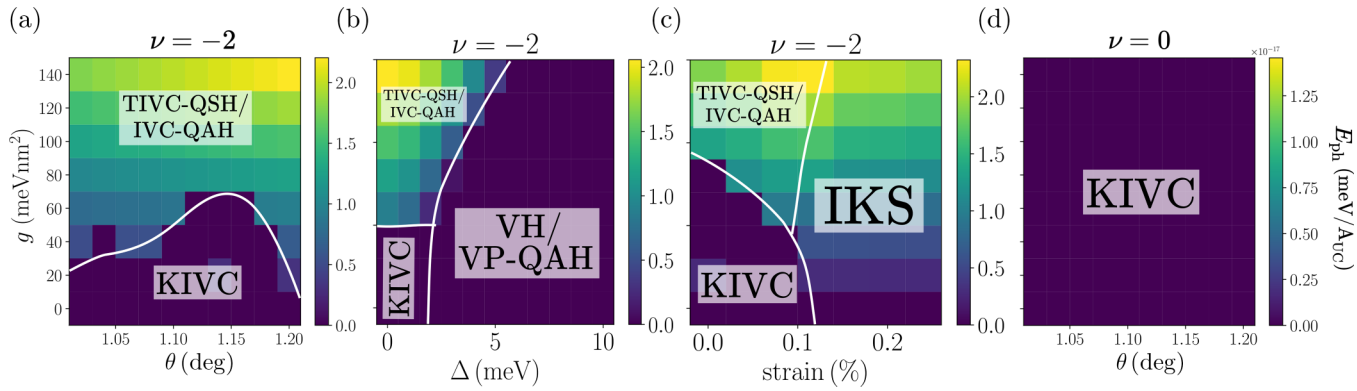

FIG. 1. Competing orders at even integer filling ν. Color shows the lattice distortion energy $E_{\rm ph}$; Kekulé charge density order is present in the electronic sector for $E_{\rm ph} \neq 0$. White lines show approximate phase boundaries. All phase diagrams computed in the graphene scheme. (a), (d) Phase diagram of electron-phonon coupling g vs twist angle θ for $|\nu| = 0, 2$ respectively. $w_{\rm AA} = 60$ meV, $w_{\rm AB} = 110$ meV. Representative band structures at $\nu = -2$ are shown in Ref. [74]. (b) Dependence on sublattice mass $\Delta\sigma_z$ applied to the bottom layer. $\theta = 1.10°$, $w_{\rm AA} = 50$ meV. (c) Dependence on heterostrain with strength ϵ, with strain axis along $\hat{x}$. $\theta = 1.12°$, $w_{\rm AA} = 77$ meV. [QAH: quantized anomalous Hall, KIVC: Kramers intervalley coherent, TIVC: time-reversal IVC, VP: valley polarized, QSH: quantum spin Hall].

However, it is unclear why TIVC becomes a competitive ground state at low strain.

Here, we show that electron-phonon coupling (EPC) provides a natural explanation for the emergence of low-strain TIVC order. To wit, the zone-corner in-plane optical phonon modes—which link the microscopic valleys—couple strongly to the Kekulé density distortion, lowering the energy of TIVC relative to KIVC. The competition is particularly transparent at strong coupling, where EPC generates a new term in the anisotropic nonlinear sigma model (NLSM) that describes selection between distinct $q = 0$ insulators. This clarifies that while small relative to the bare Coulomb scale, EPC is comparable in strength to other perturbations that move away from strong coupling. We therefore perform numerical Hartree-Fock (HF) simulations (Fig. 1) to capture this competition in the regime of intermediate coupling that appears on leaving the chiral-flat limit by tuning interlayer tunneling, strain, and twist angle. Our work shows that the strong-coupling phase structure at low strain is more nuanced than previously thought, and identifies a key role for phonons in selecting between competing interaction-driven ordered states.

II. MODEL

We study the Hamiltonian $\hat{H}_{\rm tot} = \hat{H}_{\rm BM} + \hat{H}_{\rm int} + \hat{H}_{\rm EPC} + \hat{H}_{A_1}$. Here, $\hat{H}_{\rm BM}$ is the standard single-particle Bistritzer-MacDonald (BM) model [80] that depends on the twist angle θ and sublattice-dependent hopping matrix elements $w_{\rm AB} = 110$ meV and $w_{\rm AA}$, which we will tune starting from the chiral limit $w_{\rm AA} = 0$. $\hat{H}_{\rm int}$ describes dual-gate screened Coulomb interactions $V(q) = \frac{e^2}{2\epsilon_0\epsilon_r q}\tanh qd$, with screening length $d = 25$ nm and permittivity $\epsilon_r = 10$ (see Ref. [74] for representative results using single-gate screened interactions). To avoid double counting, we choose the zero of interactions to correspond to the density of two decoupled graphene layers (the so-called "graphene" subtraction scheme), though we investigate alternatives in Ref. [74]. $\hat{H}_{\rm ph} = \hbar\omega\sum_{l\alpha\boldsymbol{q}}\hat{a}^\dagger_{l\alpha}(\boldsymbol{q})\hat{a}_{l\alpha}(\boldsymbol{q})$ describes graphene zone-corner (ZC) in-plane transverse optical phonons A_1, B_1, which couple to continuum electrons in each layer via [59,69,81–83]

$$\hat{H}_{\rm EPC} = \mathcal{F}\sum_{l\alpha}\int_{\boldsymbol{r}}\hat{\psi}^\dagger_l(\boldsymbol{r})[\hat{u}_{l\alpha}(\boldsymbol{r})\Gamma_\alpha]\hat{\psi}_l(\boldsymbol{r}) \tag{1}$$

with $\hat{u}_{l\alpha}(\boldsymbol{r}) = \mathcal{D}\sum_{\boldsymbol{q}} e^{i\boldsymbol{q}\cdot\boldsymbol{r}}[\hat{a}_{l\alpha}(\boldsymbol{q}) + \hat{a}^\dagger_{l\alpha}(-\boldsymbol{q})]$. Here, $\hat{\psi}_l(\boldsymbol{r})$ is a spinor in spin (s), valley (τ) and sublattice (σ) space, $\mathcal{F}, \mathcal{D}$ absorb various phonon parameters, and we approximate the phonon dispersion $\hbar\omega \simeq 160$ meV as constant (since the optical mode is roughly flat within the BM model cutoff). Each layer l has two degenerate ZC modes $\alpha = a, b$ with intervalley coupling matrices $\Gamma_a = \tau_x\sigma_x$, $\Gamma_b = \tau_y\sigma_x$. We define a characteristic (dimensionful) coupling

$$g = A\frac{\mathcal{F}^2\mathcal{D}^2}{\hbar\omega}, \tag{2}$$

where A is the system area. Typical estimates put $g \simeq 70$ meVnm^2 [59], but as these can vary widely [81], we will view it as a tuning parameter. $\hat{H}_{\rm tot}$ is invariant under spinless time-reversal $\hat{\mathcal{T}} = \tau_x\mathcal{K}$, $U(1)_V$ valley rotations, $SU(2)_s$ spin rotations, and D_6 point-group symmetry.

Strong electron-electron interactions lead to closely competing candidate ground states. Treating $\hat{H}_{\rm EPC}$ at mean-field level, the phonons will experience a linear bias term $\sim{\rm tr}\,\Gamma_\alpha P$, where P is the electron density matrix, and lower their energy by shifting their vacuum. The resulting energy gain from lattice distortion $E_{\rm ph} \sim g|{\rm tr}\,\Gamma_\alpha P|^2 \geqslant 0$ is quadratic in P, and, crucially, depends on the pattern of flavor symmetry breaking. For the ZC phonons of interest here, this effect is only operative for certain forms of $U(1)_V$-breaking intervalley coherence (IVC). Since at the noninteracting level, the remote bands are highly dispersive and separated by moiré gaps to the central bands, we expect the relevant electronic ordering to be concentrated in the latter. Hence, in the following, we consider $\hat{H}_{\rm tot}$ projected to the flat bands, though we caution that precise positions of phase boundaries may be sensitive to the inclusion of remote bands. Expressions for $E_{\rm ph}$ in the projected theory are given in Ref. [74].

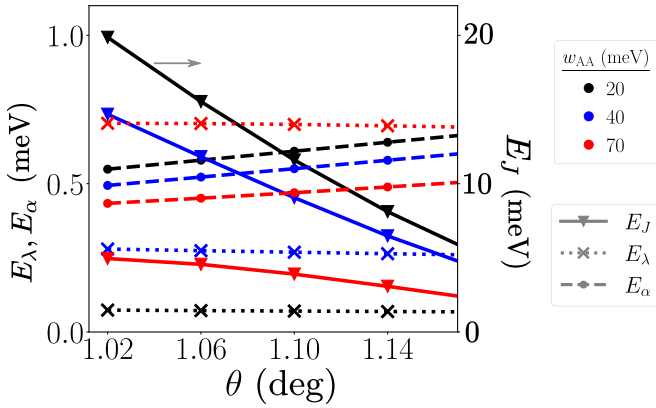

FIG. 2. Sigma model energy scales. Strong-coupling sigma model parameters for $g = 70\,\text{meVnm}^2$ in the graphene scheme. $E_\alpha = \alpha A_{UC}$ (dashed circles) measures twice the lattice distortion energy for a single intervalley coherent Chern band. Note the different scale for E_J (solid triangles).

III. STRONG-COUPLING LIMIT AND NLSM

To understand the qualitative impact of EPC on ground state selection, we first consider a nonlinear sigma model (NLSM) description [68,84,85]. In the chiral-flat limit with $\kappa = \frac{w_{AA}}{w_{AB}} = 0$ and vanishing bandwidth, we can rotate to the Chern basis which is sublattice polarized and has Chern numbers $C = \tau_z\sigma_z$ (the polarization is imperfect for $\kappa \neq 0$). At integer $\nu \equiv \nu_+ + \nu_- - 4$, the exact ground states are Slater determinants constructed by filling ν_+ bands with $C = 1$ and ν_- bands with $C = -1$, allowing arbitrary rotations within each Chern sector. These "generalized ferromagnets" spontaneously break the $U(4) \times U(4)$ symmetry of the chiral-flat limit to $U(\nu_+) \times U(4-\nu_+) \times U(\nu_-) \times U(4-\nu_-)$, which sets the NLSM target space. Deviations from the chiral-flat limit explicitly break $U(4) \times U(4)$, leading to anisotropies in the NLSM energy density

$$\mathcal{E}[Q] = \frac{J}{4}\text{tr}\,(Q\gamma_x)^2 - \frac{\lambda}{4}\text{tr}\,(Q\gamma_x\eta_z)^2 - \frac{\alpha}{8}[(\text{tr}\,Q\eta_x)^2 + (\text{tr}\,Q\eta_y)^2], \quad (3)$$

where we have defined the Pauli triplets $\gamma_{x,y,z} = (\sigma_x, \sigma_y\tau_z, \sigma_z\tau_z)$, $\eta_{x,y,z} = (\sigma_x\,\tau_x,\ \sigma_x\,\tau_y,\ \tau_z)$. $Q = \text{diag}\,(Q^+, Q^-)$ is the 8×8 single-particle density matrix. Q is block diagonal in Chern sectors $C = \pm$, which satisfies $Q^2 = 1$ and $\text{tr}\,Q = 2\nu$. J and λ are previously-computed [40,85] terms arising from inter-Chern tunneling (superexchange) and finite κ, respectively. The α term is new, and represents the phonon energy from coupling to the Kekulé charge density. We argue that its inclusion is necessary since its magnitude is comparable to the other anisotropies (Fig. 2).

In Table I, we list the candidate strong-coupling states at even integers focusing on uniform valley-unpolarized orders [86]. Prior theory has consistently favored the KIVC at even ν on the grounds that it maximally satisfies both J and λ terms [40,50]. However, despite its IVC, it does not benefit from EPC. This is due to its $\hat{\mathcal{T}}' = \tau_y\mathcal{K}$ symmetry, which forces the Kekulé charge density to vanish [78,79]. The TIVC is usually ignored due to its energy penalty under J and λ, but it can gain from the α term since the Kekulé densities of its bands interfere constructively. This could be anticipated from the phonon coupling matrices η_x, η_y in Eq. (3) which are precisely the order parameters of the TIVC. For finite chiral ratio, this effect decreases as the sublattice polarization of the Chern bands is reduced, but α remains appreciable [Fig. 2(a)].

For $|\nu| = 2$, which is of most relevance to Ref. [19], the case for TIVC is strongest, due to nontrivial interplay with spin physics. The prevailing theoretical expectation for the ground state is the spin-polarized KIVC [up to $SU_K(2) \times SU_{\bar{K}}(2)$ spin rotations]. The J and λ terms are antagonistic toward the spin-polarized TIVC. However, by flipping the spin in one Chern sector, we can construct instead a new state, the TIVC-QSH, which does not incur the energy cost J (Table I). This is because inter-Chern tunneling is no longer Pauli-blocked, allowing superexchange. Therefore, it suffices only that $\alpha > \lambda$ for this phase with Kekulé charge order to emerge; from Fig. 2 we see that these are indeed comparable. Note that the TIVC-QSH satisfies spinful time-reversal and is a quantum spin Hall insulator (hence the name). Applying spinless $\hat{\mathcal{T}}$ on one spin species produces a degenerate IVC order with $|C| = 2$ quantized anomalous Hall (QAH) response, which we dub the IVC-QAH [83]. Both this and the TIVC-QSH exhibit quantized topological responses.

At neutrality, the superexchange mechanism that stabilizes TIVC-QSH is Pauli blocked and KIVC dominates TIVC orders due to the large J, inevitably present in the graphene subtraction scheme. However, the choice of scheme influences

TABLE I. Valley-unpolarized strong-coupling states at even integer filling. All states are moiré translation symmetric. Orders at neutrality are spin unpolarized. E denotes energy in the sigma model. "Current" can refer to charge and spin currents. $*$ indicates a degenerate manifold of states obtained via valley-resolved $SU_S(2)$ rotation. Density matrices Q are shown in Ref. [74]. VH: valley Hall.

Phase	$\|\nu\|$	$\|\psi\rangle$	E	Kekulé	C	Spin pol.
KIVC	0	$(\|KA\rangle + \|\bar{K}B\rangle)(\|KB\rangle - \|\bar{K}A\rangle)$	$-2J - 2\lambda$	Current	0	0
TIVC	0	$(\|KA\rangle + \|\bar{K}B\rangle)(\|KB\rangle + \|\bar{K}A\rangle)$	$2J + 2\lambda - 8\alpha$	Charge	0	0
VH	0	$\|KA\rangle\,\|\bar{K}A\rangle$	$-2J + 2\lambda$	✗	0	0
KIVC	2	$(\|KA\uparrow\rangle + \|\bar{K}B\uparrow\rangle)(\|KB\uparrow\rangle - \|\bar{K}A\uparrow\rangle)$	-2λ	Current	0	*
TIVC-SP	2	$(\|KA\uparrow\rangle + \|\bar{K}B\uparrow\rangle)(\|KB\uparrow\rangle + \|\bar{K}A\uparrow\rangle)$	$2J - 2\alpha$	Charge	0	2
TIVC-QSH	2	$(\|KA\uparrow\rangle + \|\bar{K}B\uparrow\rangle)(\|KB\downarrow\rangle + \|\bar{K}A\downarrow\rangle)$	-2α	Charge	0	0
IVC-QAH	2	$(\|KA\uparrow\rangle + \|\bar{K}B\uparrow\rangle)(\|KA\downarrow\rangle + \|\bar{K}B\downarrow\rangle)$	-2α	Charge	2	0
VH	2	$\|KA\uparrow\rangle\,\|\bar{K}A\uparrow\rangle$	0	✗	0	*

the interaction-renormalized bandwidth, with a particularly strong effect on J. In the "average" scheme [74], $J = \lambda = 0$ at the magic angle in the chiral-flat limit, ensuring Kekulé charge order for any $\alpha > 0$ [74]; away from this limit, J remains small, suggesting a qualitatively different $\nu = 0$ phase diagram.

IV. HARTREE-FOCK RESULTS

To study the phase competition beyond the NLSM, we perform HF calculations for a realistic chiral ratio. Phonons are included self-consistently by optimizing over products of electronic Slater determinants and phonon coherent states. We assume moiré translation symmetry and diagonal spin structure. Since our model has approximate particle-hole symmetry [87–89], we only show data for $\nu \leqslant 0$.

At $\nu = -2$, the ground state is the KIVC for small values of g (Fig. 1). As expected from its $\hat{\mathcal{T}}'$ symmetry, it has vanishing Kekulé charge density and does not couple linearly to the ZC phonons. For larger EPC, we find a first-order transition to a gapped phase with finite Kekulé charge order, which either satisfies spinful TRS (TIVC-QSH) or is a $|C| = 2$ Chern insulator (IVC-QAH). These are degenerate at HF level, exhibit identical Kekulé patterns, and possess nearly perfect IVC across the moiré Brillouin zone (mBZ). The fact that $E_{\text{ph}} \approx 2E_\alpha$ [Fig. 2(a)] strongly suggests that these states are quantitatively similar to those in the NLSM limit.

At $\nu = 0$, we find only KIVC order for the same parameter window, with no competing Kekulé charge orders.

We also study the phase diagrams for odd ν [74]. For a single Chern band, the anisotropy that selects valley polarization over IVC is much smaller than the terms in Eq. (3) [50]. Therefore, the transition to states with Kekulé charge density occurs for weaker EPC.

Finally, we comment that in the average scheme [74] at $\nu = 0$, a first-order KIVC-TIVC transition with increasing g reappears, whereas the phase boundaries at $|\nu| \geqslant 2$ are largely unchanged. These observations are consistent with the NLSM discussion above.

Alignment of MA-TBG to the hBN substrate breaks $\hat{C}_{2z}$ symmetry, and can be modeled via a sublattice mass $\Delta\sigma_z$ [63,90,91] (though there are likely additional complicated effects [20,92–100]). As shown in Fig. 1(b) for $\nu = -2$, the sublattice bias competes with intervalley coherence, and both IVC orders give way to the valley Hall (VH) phase for modest values of Δ. This is a smooth crossover between states on the pseudospin Bloch sphere, driven by the sublattice potential.

In the EPC-heterostrain phase diagram at $\nu = -2$ [Fig. 1(c)], all three types of IVC ordering are present. The band gaps of the moiré translation invariant ($q = 0$) TIVC and KIVC are rapidly suppressed by strain [54,65], yielding to IKS for small strains typical of most MA-TBG devices. Since the IKS possesses Kekulé bond order, it can directly couple to the ZC phonons, thereby explaining its relative stability against the TIVC for finite g. The IKS can be sharply distinguished from the TIVC by its nonzero q, trivial spin Chern number, and strongly inhomogeneous IVC in momentum space [54,101].

V. DISCUSSION

While virtual phonons in MA-TBG have previously been invoked to explain superconductivity [59–62,102–104] and resolve spin degeneracies via Hund's coupling [23,69,105–107], the role played by zone-corner optical phonons here is special: by triggering a physical lattice distortion in response to electronic Kekulé charge order, phonons directly participate in ground state selection. This modifies the physics to the extent that the TIVC, usually considered the least likely strong-coupling order, can emerge as the ground state at even integer ν. This "valley Jahn-Teller effect" [82] has been previously studied using HF and projected resonating-valence bond (RVB) wavefunctions [83]. However, while Ref. [83] did find that KIVC becomes unstable to Kekulé charge order, it did not consider competition with translational-breaking orders like IKS in the presence of strain or substrate alignment, nor, crucially, did it apply the lens of the strong coupling NLSM as we do here. Hence, Ref. [83] identified the IVC-QAH state as the only possible alternative to KIVC at $\nu = -2$. In contrast, our NLSM analysis shows that TIVC-QSH and IVC-QAH are degenerate (certainly at HF level but possibly beyond). TIVC-QSH is more consistent with the bulk of experiments, which do not see QAH at $|\nu| = 2$, and we find that it is suppressed at moderate strain in favor of IKS, consistent with experiments [19]. On a more technical level, we note that Ref. [83] used an unusual subtraction scheme, wherein Kekulé charge order appears roughly equally stable at $|\nu| = 0, 2$, in contrast to our graphene-scheme results where it appears to be weaker at neutrality—again, in potential agreement with experiments [19].

Beyond offering a resolution to an immediate experimental puzzle [19], the emergence of TIVC has ramifications for other aspects of correlation physics in moiré graphene. It has been argued that experiments in MA-TBG and TTG indicate pairing between opposite spins and valleys in the superconducting dome commonly observed upon hole doping $\nu = -2$ [105]. Both TIVC-QSH and IKS preserve spinful TRS and accommodate such pairing (unlike KIVC or IVC-QAH). The absence of spin polarization is already established at an energy above the weak Hund's coupling [23], whose sign is difficult to compute [69].

The topology of the TIVC leads to phenomena distinct from the IKS. Topological spin/pseudospin textures are charged, and may pair if the energetics are favorable [68,85,108]. At $|\nu| = 2$, the TIVC-QSH exhibits a quantum spin Hall effect protected by S_z conservation. Crucially, boundaries do not gap the edge modes, unlike the KIVC where the protecting $\hat{\mathcal{T}}'$ symmetry is broken by scattering at edges [40]. The TRS-violating IVC-QAH could explain [83] experiments which see time-reversal symmetry breaking at $|\nu| = 2$ [24,29], without substrate coupling.

Optical phonon distortion is likely relevant to TTG as well, whose bands resemble MA-TBG except for extra dispersive Dirac cones. TTG is phenomenologically similar to MA-TBG, e.g., it also hosts superconducting domes proximate to correlated insulators [109–114]. TTG has been observed to form solitons [115], suggesting the emergence of low-strain regions ideal for realizing this phonon-induced selection of electronic order. We speculate that intervalley

phonons may also influence the phase structure of correlated moiréless graphene multilayers, which exhibit multiple Fermi surface reconstructions and flavor symmetry-breaking transitions [116–122], though the intralayer intersublattice EPC is suppressed in Bernal-stacked structures [123].

We have focused on optical zone-corner phonons since they directly couple to IVC order. There is a plethora of other phonons, from optical zone-center modes to low-energy moiré acoustic phonons and phasons [82,103,123–133]. Incorporation of additional terms [134–136] in the BM model would be useful to refine the single-particle Hamiltonian and recover the particle-hole symmetry breaking seen in experiments. It may also be interesting to examine the role of ZC EPC in heavy fermion formulations of MA-TBG and TTG [137–139].

ACKNOWLEDGMENTS

We thank S. Kivelson for useful discussions and A. Yazdani and the authors of Ref. [19] for sharing their results with us shortly before their publication. We acknowledge support from the European Research Council (ERC) under the European Union Horizon 2020 Research and Innovation Programme (Grant Agreements No. 804213-TMCS, No. 757867-PARATOP, and No. 817799-HQMAT) and from EPSRC Grant No. EP/S020527/1.

[1] Y. Cao, V. Fatemi, A. Demir, S. Fang, S. L. Tomarken, J. Y. Luo, J. D. Sanchez-Yamagishi, K. Watanabe, T. Taniguchi, E. Kaxiras, R. C. Ashoori, and P. Jarillo-Herrero, Correlated insulator behaviour at half-filling in magic-angle graphene superlattices, Nature (London) **556**, 80 (2018).

[2] Y. Cao, V. Fatemi, S. Fang, K. Watanabe, T. Taniguchi, E. Kaxiras, and P. Jarillo-Herrero, Unconventional superconductivity in magic-angle graphene superlattices, Nature (London) **556**, 43 (2018).

[3] M. Yankowitz, S. Chen, H. Polshyn, Y. Zhang, K. Watanabe, T. Taniguchi, D. Graf, A. F. Young, and C. R. Dean, Tuning superconductivity in twisted bilayer graphene, Science **363**, 1059 (2019).

[4] X. Lu, P. Stepanov, W. Yang, M. Xie, M. A. Aamir, I. Das, C. Urgell, K. Watanabe, T. Taniguchi, G. Zhang, A. Bachtold, A. H. MacDonald, and D. K. Efetov, Superconductors, orbital magnets and correlated states in magic-angle bilayer graphene, Nature (London) **574**, 653 (2019).

[5] J. M. Park, Y. Cao, K. Watanabe, T. Taniguchi, and P. Jarillo-Herrero, Flavour Hund's coupling, Chern gaps and charge diffusivity in moiré graphene, Nature (London) **592**, 43 (2021).

[6] U. Zondiner, A. Rozen, D. Rodan-Legrain, Y. Cao, R. Queiroz, T. Taniguchi, K. Watanabe, Y. Oreg, F. von Oppen, A. Stern *et al.*, Cascade of phase transitions and Dirac revivals in magic-angle graphene, Nature (London) **582**, 203 (2020).

[7] A. Uri, S. Grover, Y. Cao, J. A. Crosse, K. Bagani, D. Rodan-Legrain, Y. Myasoedov, K. Watanabe, T. Taniguchi, P. Moon *et al.*, Mapping the twist-angle disorder and Landau levels in magic-angle graphene, Nature (London) **581**, 47 (2020).

[8] Y. Saito, J. Ge, K. Watanabe, T. Taniguchi, and A. F. Young, Independent superconductors and correlated insulators in twisted bilayer graphene, Nat. Phys. **16**, 926 (2020).

[9] Y. Saito, F. Yang, J. Ge, X. Liu, T. Taniguchi, K. Watanabe, J. Li, E. Berg, and A. F. Young, Isospin Pomeranchuk effect in twisted bilayer graphene, Nature (London) **592**, 220 (2021).

[10] Y. Cao, D. Rodan-Legrain, J. M. Park, N. F. Q. Yuan, K. Watanabe, T. Taniguchi, R. M. Fernandes, L. Fu, and P. Jarillo-Herrero, Nematicity and competing orders in superconducting magic-angle graphene, Science **372**, 264 (2021).

[11] X. Liu, Z. Wang, K. Watanabe, T. Taniguchi, O. Vafek, and J. Li, Tuning electron correlation in magic-angle twisted bilayer graphene using Coulomb screening, Science **371**, 1261 (2021).

[12] I. Das, X. Lu, J. Herzog-Arbeitman, Z.-D. Song, K. Watanabe, T. Taniguchi, B. A. Bernevig, and D. K. Efetov, Symmetry-broken Chern insulators and Rashba-like Landau-level crossings in magic-angle bilayer graphene, Nat. Phys. **17**, 710 (2021).

[13] A. Rozen, J. M. Park, U. Zondiner, Y. Cao, D. Rodan-Legrain, T. Taniguchi, K. Watanabe, Y. Oreg, A. Stern, E. Berg *et al.*, Entropic evidence for a Pomeranchuk effect in magic-angle graphene, Nature (London) **592**, 214 (2021).

[14] M. Serlin, C. L. Tschirhart, H. Polshyn, Y. Zhang, J. Zhu, K. Watanabe, T. Taniguchi, L. Balents, and A. F. Young, Intrinsic quantized anomalous Hall effect in a moiré heterostructure, Science **367**, 900 (2020).

[15] A. L. Sharpe, E. J. Fox, A. W. Barnard, J. Finney, K. Watanabe, T. Taniguchi, M. A. Kastner, and D. Goldhaber-Gordon, Emergent ferromagnetism near three-quarters filling in twisted bilayer graphene, Science **365**, 605 (2019).

[16] P. Stepanov, I. Das, X. Lu, A. Fahimniya, K. Watanabe, T. Taniguchi, F. H. L. Koppens, J. Lischner, L. Levitov, and D. K. Efetov, Untying the insulating and superconducting orders in magic-angle graphene, Nature (London) **583**, 375 (2020).

[17] S. Wu, Z. Zhang, K. Watanabe, T. Taniguchi, and E. Y. Andrei, Chern insulators, Van Hove singularities and topological flat bands in magic-angle twisted bilayer graphene, Nat. Mater. **20**, 488 (2021).

[18] Y. Saito, J. Ge, L. Rademaker, K. Watanabe, T. Taniguchi, D. A. Abanin, and A. F. Young, Hofstadter subband ferromagnetism and symmetry-broken Chern insulators in twisted bilayer graphene, Nat. Phys. **17**, 478 (2021).

[19] K. P. Nuckolls, R. L. Lee, M. Oh, D. Wong, T. Soejima, J. P. Hong, D. Călugăru, J. Herzog-Arbeitman, B. A. Bernevig, K. Watanabe, T. Taniguchi, N. Regnault, M. P. Zaletel, and A. Yazdani, Quantum textures of the many-body wavefunctions in magic-angle graphene, Nature (London) **620**, 525 (2023).

[20] S. Grover, M. Bocarsly, A. Uri, P. Stepanov, G. D. Battista, I. Roy, J. Xiao, A. Y. Meltzer, Y. Myasoedov, K. Pareek, K. Watanabe, T. Taniguchi, B. Yan, A. Stern, E. Berg, D. K. Efetov, and E. Zeldov, Chern mosaic and Berry-curvature magnetism in magic-angle graphene, Nat. Phys. **18**, 885 (2022).

[21] J. Yu, B. A. Foutty, Z. Han, M. E. Barber, Y. Schattner, K. Watanabe, T. Taniguchi, P. Phillips, Z.-X. Shen, S. A. Kivelson, and B. E. Feldman, Correlated Hofstadter spectrum

and flavour phase diagram in magic-angle twisted bilayer graphene, Nat. Phys. **18**, 825 (2022).

[22] J. Yu, B. A. Foutty, Y. H. Kwan, M. E. Barber, K. Watanabe, T. Taniguchi, Z.-X. Shen, S. A. Parameswaran, and B. E. Feldman, Spin skyrmion gaps as signatures of intervalley-coherent insulators in magic-angle twisted bilayer graphene, Nat. Commun. **14**, 6679 (2023).

[23] E. Morissette, J.-X. Lin, D. Sun, L. Zhang, S. Liu, D. Rhodes, K. Watanabe, T. Taniguchi, J. Hone, J. Pollanen, M. S. Scheurer, M. Lilly, A. Mounce, and J. I. A. Li, Electron spin resonance and collective excitations in magic-angle twisted bilayer graphene, Nat. Phys. **19**, 1156 (2023).

[24] C.-C. Tseng, X. Ma, Z. Liu, K. Watanabe, T. Taniguchi, J.-H. Chu, and M. Yankowitz, Anomalous Hall effect at half filling in twisted bilayer graphene, Nat. Phys. **18**, 1038 (2022).

[25] Y. Choi, J. Kemmer, Y. Peng, A. Thomson, H. Arora, R. Polski, Y. Zhang, H. Ren, J. Alicea, G. Refael *et al.*, Electronic correlations in twisted bilayer graphene near the magic angle, Nat. Phys. **15**, 1174 (2019).

[26] M. Oh, K. P. Nuckolls, D. Wong, R. L. Lee, X. Liu, K. Watanabe, T. Taniguchi, and A. Yazdani, Evidence for unconventional superconductivity in twisted bilayer graphene, Nature (London) **600**, 240 (2021).

[27] K. P. Nuckolls, M. Oh, D. Wong, B. Lian, K. Watanabe, T. Taniguchi, B. A. Bernevig, and A. Yazdani, Strongly correlated Chern insulators in magic-angle twisted bilayer graphene, Nature (London) **588**, 610 (2020).

[28] Y. Xie, A. T. Pierce, J. M. Park, D. E. Parker, E. Khalaf, P. Ledwith, Y. Cao, S. H. Lee, S. Chen, P. R. Forrester, K. Watanabe, T. Taniguchi, A. Vishwanath, P. Jarillo-Herrero, and A. Yacoby, Fractional Chern insulators in magic-angle twisted bilayer graphene, Nature (London) **600**, 439 (2021).

[29] J. Diez-Merida, A. Diez-Carlon, S. Y. Yang, Y. M. Xie, X. J. Gao, K. Watanabe, T. Taniguchi, X. Lu, K. T. Law, and D. K. Efetov, Magnetic Josephson junctions and superconducting diodes in magic angle twisted bilayer graphene, Nat Commun **14**, 2396 (2023).

[30] Y. Jiang, X. Lai, K. Watanabe, T. Taniguchi, K. Haule, J. Mao, and E. Y. Andrei, Charge order and broken rotational symmetry in magic-angle twisted bilayer graphene, Nature (London) **573**, 91 (2019).

[31] H. S. Arora, R. Polski, Y. Zhang, A. Thomson, Y. Choi, H. Kim, Z. Lin, I. Z. Wilson, X. Xu, J.-H. Chu, K. Watanabe, T. Taniguchi, J. Alicea, and S. Nadj-Perge, Superconductivity in metallic twisted bilayer graphene stabilized by WSe_2, Nature (London) **583**, 379 (2020).

[32] A. Kerelsky, L. J. McGilly, D. M. Kennes, L. Xian, M. Yankowitz, S. Chen, K. Watanabe, T. Taniguchi, J. Hone, C. Dean *et al.*, Maximized electron interactions at the magic angle in twisted bilayer graphene, Nature (London) **572**, 95 (2019).

[33] Y. Choi, H. Kim, Y. Peng, A. Thomson, C. Lewandowski, R. Polski, Y. Zhang, H. S. Arora, K. Watanabe, T. Taniguchi *et al.*, Correlation-driven topological phases in magic-angle twisted bilayer graphene, Nature (London) **589**, 536 (2021).

[34] Y. Xie, B. Lian, B. Jäck, X. Liu, C.-L. Chiu, K. Watanabe, T. Taniguchi, B. A. Bernevig, and A. Yazdani, Spectroscopic signatures of many-body correlations in magic angle twisted bilayer graphene, Nature (London) **572**, 101 (2019).

[35] D. Wong, K. P. Nuckolls, M. Oh, B. Lian, Y. Xie, S. Jeon, K. Watanabe, T. Taniguchi, B. A. Bernevig, and A. Yazdani, Cascade of electronic transitions in magic-angle twisted bilayer graphene, Nature (London) **582**, 198 (2020).

[36] A. T. Pierce, Y. Xie, J. M. Park, E. Khalaf, S. H. Lee, Y. Cao, D. E. Parker, P. R. Forrester, S. Chen, K. Watanabe, T. Taniguchi, A. Vishwanath, P. Jarillo-Herrero, and A. Yacoby, Unconventional sequence of correlated Chern insulators in magic-angle twisted bilayer graphene, Nat. Phys. **17**, 1210 (2021).

[37] H. C. Po, L. Zou, A. Vishwanath, and T. Senthil, Origin of Mott insulating behavior and superconductivity in twisted bilayer graphene, Phys. Rev. X **8**, 031089 (2018).

[38] M. Xie and A. H. MacDonald, Weak-field Hall resistivity and spin-valley flavor symmetry breaking in magic-angle twisted bilayer graphene, Phys. Rev. Lett. **127**, 196401 (2021).

[39] M. Xie and A. H. MacDonald, Nature of the correlated insulator states in twisted bilayer graphene, Phys. Rev. Lett. **124**, 097601 (2020).

[40] N. Bultinck, E. Khalaf, S. Liu, S. Chatterjee, A. Vishwanath, and M. P. Zaletel, Ground state and hidden symmetry of magic-angle graphene at even integer filling, Phys. Rev. X **10**, 031034 (2020).

[41] J. Liu and X. Dai, Theories for the correlated insulating states and quantum anomalous Hall effect phenomena in twisted bilayer graphene, Phys. Rev. B **103**, 035427 (2021).

[42] T. Cea and F. Guinea, Band structure and insulating states driven by Coulomb interaction in twisted bilayer graphene, Phys. Rev. B **102**, 045107 (2020).

[43] Y. Zhang, K. Jiang, Z. Wang, and F. Zhang, Correlated insulating phases of twisted bilayer graphene at commensurate filling fractions: A Hartree-Fock study, Phys. Rev. B **102**, 035136 (2020).

[44] M. Ochi, M. Koshino, and K. Kuroki, Possible correlated insulating states in magic-angle twisted bilayer graphene under strongly competing interactions, Phys. Rev. B **98**, 081102(R) (2018).

[45] J. Kang and O. Vafek, Strong coupling phases of partially filled twisted bilayer graphene narrow bands, Phys. Rev. Lett. **122**, 246401 (2019).

[46] J. Kang and O. Vafek, Non-Abelian Dirac node braiding and near-degeneracy of correlated phases at odd integer filling in magic-angle twisted bilayer graphene, Phys. Rev. B **102**, 035161 (2020).

[47] O. Vafek and J. Kang, Renormalization group study of hidden symmetry in twisted bilayer graphene with Coulomb interactions, Phys. Rev. Lett. **125**, 257602 (2020).

[48] S. Liu, E. Khalaf, J. Y. Lee, and A. Vishwanath, Nematic topological semimetal and insulator in magic-angle bilayer graphene at charge neutrality, Phys. Rev. Res. **3**, 013033 (2021).

[49] J. F. Dodaro, S. A. Kivelson, Y. Schattner, X. Q. Sun, and C. Wang, Phases of a phenomenological model of twisted bilayer graphene, Phys. Rev. B **98**, 075154 (2018).

[50] B. Lian, Z.-D. Song, N. Regnault, D. K. Efetov, A. Yazdani, and B. A. Bernevig, Twisted bilayer graphene. IV. Exact insulator ground states and phase diagram, Phys. Rev. B **103**, 205414 (2021).

[51] B. A. Bernevig, B. Lian, A. Cowsik, F. Xie, N. Regnault, and Z.-D. Song, Twisted bilayer graphene. V. exact analytic

many-body excitations in Coulomb Hamiltonians: Charge gap, goldstone modes, and absence of Cooper pairing, Phys. Rev. B **103**, 205415 (2021).

[52] F. Xie, A. Cowsik, Z.-D. Song, B. Lian, B. A. Bernevig, and N. Regnault, Twisted bilayer graphene. VI. An exact diagonalization study at nonzero integer filling, Phys. Rev. B **103**, 205416 (2021).

[53] T. Soejima, D. E. Parker, N. Bultinck, J. Hauschild, and M. P. Zaletel, Efficient simulation of moiré materials using the density matrix renormalization group, Phys. Rev. B **102**, 205111 (2020).

[54] Y. H. Kwan, G. Wagner, T. Soejima, M. P. Zaletel, S. H. Simon, S. A. Parameswaran, and N. Bultinck, Kekulé spiral order at all nonzero integer fillings in twisted bilayer graphene, Phys. Rev. X **11**, 041063 (2021).

[55] P. Potasz, M. Xie, and A. H. MacDonald, Exact diagonalization for magic-angle twisted bilayer graphene, Phys. Rev. Lett. **127**, 147203 (2021).

[56] X. Zhang, G. Pan, Y. Zhang, J. Kang, and Z. Y. Meng, Momentum space quantum Monte Carlo on twisted bilayer graphene, Chin. Phys. Lett. **38**, 077305 (2021).

[57] L. Klebl, Z. A. H. Goodwin, A. A. Mostofi, D. M. Kennes, and J. Lischner, Importance of long-ranged electron-electron interactions for the magnetic phase diagram of twisted bilayer graphene, Phys. Rev. B **103**, 195127 (2021).

[58] G. Shavit, E. Berg, A. Stern, and Y. Oreg, Theory of correlated insulators and superconductivity in twisted bilayer graphene, Phys. Rev. Lett. **127**, 247703 (2021).

[59] F. Wu, A. H. MacDonald, and I. Martin, Theory of phonon-mediated superconductivity in twisted bilayer graphene, Phys. Rev. Lett. **121**, 257001 (2018).

[60] B. Lian, Z. Wang, and B. A. Bernevig, Twisted bilayer graphene: A phonon-driven superconductor, Phys. Rev. Lett. **122**, 257002 (2019).

[61] F. Wu, E. Hwang, and S. Das Sarma, Phonon-induced giant linear-in-T resistivity in magic angle twisted bilayer graphene: Ordinary strangeness and exotic superconductivity, Phys. Rev. B **99**, 165112 (2019).

[62] C. Lewandowski, D. Chowdhury, and J. Ruhman, Pairing in magic-angle twisted bilayer graphene: Role of phonon and plasmon umklapp, Phys. Rev. B **103**, 235401 (2021).

[63] N. Bultinck, S. Chatterjee, and M. P. Zaletel, Mechanism for anomalous Hall ferromagnetism in twisted bilayer graphene, Phys. Rev. Lett. **124**, 166601 (2020).

[64] K. Hejazi, X. Chen, and L. Balents, Hybrid wannier Chern bands in magic angle twisted bilayer graphene and the quantized anomalous Hall effect, Phys. Rev. Res. **3**, 013242 (2021).

[65] D. E. Parker, T. Soejima, J. Hauschild, M. P. Zaletel, and N. Bultinck, Strain-induced quantum phase transitions in magic-angle graphene, Phys. Rev. Lett. **127**, 027601 (2021).

[66] A. Thomson and J. Alicea, Recovery of massless Dirac fermions at charge neutrality in strongly interacting twisted bilayer graphene with disorder, Phys. Rev. B **103**, 125138 (2021).

[67] M. Christos, S. Sachdev, and M. S. Scheurer, Superconductivity, correlated insulators, and Wess–Zumino–Witten terms in twisted bilayer graphene, Proc. Natl. Acad. Sci. USA **117**, 29543 (2020).

[68] E. Khalaf, S. Chatterjee, N. Bultinck, M. P. Zaletel, and A. Vishwanath, Charged skyrmions and topological origin of superconductivity in magic-angle graphene, Sci. Adv. **7**, eabf5299 (2021).

[69] S. Chatterjee, N. Bultinck, and M. P. Zaletel, Symmetry breaking and skyrmionic transport in twisted bilayer graphene, Phys. Rev. B **101**, 165141 (2020).

[70] T. Cea, P. A. Pantaleón, N. R. Walet, and F. Guinea, Electrostatic interactions in twisted bilayer graphene, Nano Mater. Sci. **4**, 27 (2022).

[71] Z. A. H. Goodwin, V. Vitale, X. Liang, A. A. Mostofi, and J. Lischner, Hartree theory calculations of quasiparticle properties in twisted bilayer graphene, Electron. Struct. **2**, 034001 (2020).

[72] Z. A. H. Goodwin, V. Vitale, F. Corsetti, D. K. Efetov, A. A. Mostofi, and J. Lischner, Critical role of device geometry for the phase diagram of twisted bilayer graphene, Phys. Rev. B **101**, 165110 (2020).

[73] G. Tarnopolsky, A. J. Kruchkov, and A. Vishwanath, Origin of magic angles in twisted bilayer graphene, Phys. Rev. Lett. **122**, 106405 (2019).

[74] See Supplemental Material http://link.aps.org/supplemental/10.1103/PhysRevB.110.085160 to this article for detailed expressions of the lattice distortion energy and additional numerical results in the average subtraction scheme.

[75] F. Xie, J. Kang, B. A. Bernevig, O. Vafek, and N. Regnault, Phase diagram of twisted bilayer graphene at filling factor $\nu = \pm 3$, Phys. Rev. B **107**, 075156 (2023).

[76] G. Wagner, Y. H. Kwan, N. Bultinck, S. H. Simon, and S. A. Parameswaran, Global phase diagram of the normal state of twisted bilayer graphene, Phys. Rev. Lett. **128**, 156401 (2022).

[77] H. Kim, Y. Choi, É. Lantagne-Hurtubise, C. Lewandowski, A. Thomson, L. Kong, H. Zhou, E. Baum, Y. Zhang, L. Holleis *et al.*, Imaging inter-valley coherent order in magic-angle twisted trilayer graphene, Nature (London) **623**, 942 (2023).

[78] D. Călugăru, N. Regnault, M. Oh, K. P. Nuckolls, D. Wong, R. L. Lee, A. Yazdani, O. Vafek, and B. A. Bernevig, Spectroscopy of twisted bilayer graphene correlated insulators, Phys. Rev. Lett. **129**, 117602 (2022).

[79] J. P. Hong, T. Soejima, and M. P. Zaletel, Detecting symmetry breaking in magic angle graphene using scanning tunneling microscopy, Phys. Rev. Lett. **129**, 147001 (2022).

[80] R. Bistritzer and A. H. MacDonald, Moiré bands in twisted double-layer graphene, Proc. Natl. Acad. Sci. USA **108**, 12233 (2011).

[81] D. M. Basko and I. L. Aleiner, Interplay of Coulomb and electron-phonon interactions in graphene, Phys. Rev. B **77**, 041409(R) (2008).

[82] M. Angeli, E. Tosatti, and M. Fabrizio, Valley Jahn-Teller effect in twisted bilayer graphene, Phys. Rev. X **9**, 041010 (2019).

[83] A. Blason and M. Fabrizio, Local Kekulé distortion turns twisted bilayer graphene into topological Mott insulators and superconductors, Phys. Rev. B **106**, 235112 (2022).

[84] E. Khalaf, N. Bultinck, A. Vishwanath, and M. P. Zaletel, Soft modes in magic angle twisted bilayer graphene, arXiv:2009.14827.

[85] Y. H. Kwan, G. Wagner, N. Bultinck, S. H. Simon, and S. A. Parameswaran, Skyrmions in twisted bilayer graphene: Stability, pairing, and crystallization, Phys. Rev. X **12**, 031020 (2022).

[86] Note that the expressions for certain states differ from those in Ref. [40] due to an overall constant energy shift, a different normalization for the sigma model, and the inclusion of spin.
[87] L. Zou, H. C. Po, A. Vishwanath, and T. Senthil, Band structure of twisted bilayer graphene: Emergent symmetries, commensurate approximants, and wannier obstructions, Phys. Rev. B **98**, 085435 (2018).
[88] Z. Song, Z. Wang, W. Shi, G. Li, C. Fang, and B. A. Bernevig, All magic angles in twisted bilayer graphene are topological, Phys. Rev. Lett. **123**, 036401 (2019).
[89] K. Hejazi, C. Liu, H. Shapourian, X. Chen, and L. Balents, Multiple topological transitions in twisted bilayer graphene near the first magic angle, Phys. Rev. B **99**, 035111 (2019).
[90] J. Jung, A. M. DaSilva, A. H. MacDonald, and S. Adam, Origin of band gaps in graphene on hexagonal boron nitride, Nat. Commun. **6**, 6308 (2015).
[91] Y.-H. Zhang, D. Mao, and T. Senthil, Twisted bilayer graphene aligned with hexagonal boron nitride: Anomalous Hall effect and a lattice model, Phys. Rev. Res. **1**, 033126 (2019).
[92] M. Long, P. A. Pantaleón, Z. Zhan, F. Guinea, J. Á. Silva-Guillén, and S. Yuan, An atomistic approach for the structural and electronic properties of twisted bilayer graphene-boron nitride heterostructures, npj Comput. Mater. **8**, 73 (2022).
[93] T. Cea, P. A. Pantaleón, and F. Guinea, Band structure of twisted bilayer graphene on hexagonal boron nitride, Phys. Rev. B **102**, 155136 (2020).
[94] D. Mao and T. Senthil, Quasiperiodicity, band topology, and moiré graphene, Phys. Rev. B **103**, 115110 (2021).
[95] J. Shin, Y. Park, B. L. Chittari, J.-H. Sun, and J. Jung, Electron-hole asymmetry and band gaps of commensurate double moire patterns in twisted bilayer graphene on hexagonal boron nitride, Phys. Rev. B **103**, 075423 (2021).
[96] J. Shi, J. Zhu, and A. H. MacDonald, Moiré commensurability and the quantum anomalous Hall effect in twisted bilayer graphene on hexagonal boron nitride, Phys. Rev. B **103**, 075122 (2021).
[97] X. Lin, K. Su, and J. Ni, Misalignment instability in magic-angle twisted bilayer graphene on hexagonal boron nitride, 2D Mater. **8**, 025025 (2021).
[98] X. Lin and J. Ni, Symmetry breaking in the double moiré superlattices of relaxed twisted bilayer graphene on hexagonal boron nitride, Phys. Rev. B **102**, 035441 (2020).
[99] Y. H. Kwan, G. Wagner, N. Chakraborty, S. H. Simon, and S. A. Parameswaran, Domain wall competition in the Chern insulating regime of twisted bilayer graphene, Phys. Rev. B **104**, 115404 (2021).
[100] D. Wong, K. P. Nuckolls, M. Oh, R. L. Lee, K. Watanabe, T. Taniguchi, and A. Yazdani, Insulators at fractional fillings in twisted bilayer graphene partially aligned to hexagonal boron nitride, Low Temp. Phys. **49**, 655 (2023).
[101] T. Wang, D. E. Parker, T. Soejima, J. Hauschild, S. Anand, N. Bultinck, and M. P. Zaletel, Kekulé spiral order in magic-angle graphene: A density matrix renormalization group study, Phys. Rev. B **108**, 235128 (2023).
[102] T. Cea and F. Guinea, Coulomb interaction, phonons, and superconductivity in twisted bilayer graphene, Proc. Natl. Acad. Sci. USA **118**, e2107874118 (2021).
[103] Y. W. Choi and H. J. Choi, Strong electron-phonon coupling, electron-hole asymmetry, and nonadiabaticity in magic-angle twisted bilayer graphene, Phys. Rev. B **98**, 241412(R) (2018).
[104] T. J. Peltonen, R. Ojajärvi, and T. T. Heikkilä, Mean-field theory for superconductivity in twisted bilayer graphene, Phys. Rev. B **98**, 220504(R) (2018).
[105] E. Lake, A. S. Patri, and T. Senthil, Pairing symmetry of twisted bilayer graphene: A phenomenological synthesis, Phys. Rev. B **106**, 104506 (2022).
[106] E. Lake and T. Senthil, Reentrant superconductivity through a quantum Lifshitz transition in twisted trilayer graphene, Phys. Rev. B **104**, 174505 (2021).
[107] E. Khalaf, P. Ledwith, and A. Vishwanath, Symmetry constraints on superconductivity in twisted bilayer graphene: Fractional vortices, 4*e* condensates, or nonunitary pairing, Phys. Rev. B **105**, 224508 (2022).
[108] S. Chatterjee, M. Ippoliti, and M. P. Zaletel, Skyrmion superconductivity: DMRG evidence for a topological route to superconductivity, Phys. Rev. B **106**, 035421 (2022).
[109] Y. Cao, J. M. Park, K. Watanabe, T. Taniguchi, and P. Jarillo-Herrero, Pauli-limit violation and re-entrant superconductivity in moiré graphene, Nature (London) **595**, 526 (2021).
[110] J. M. Park, Y. Cao, K. Watanabe, T. Taniguchi, and P. Jarillo-Herrero, Tunable strongly coupled superconductivity in magic-angle twisted trilayer graphene, Nature (London) **590**, 249 (2021).
[111] Z. Hao, A. M. Zimmerman, P. Ledwith, E. Khalaf, D. H. Najafabadi, K. Watanabe, T. Taniguchi, A. Vishwanath, and P. Kim, Electric field–tunable superconductivity in alternating-twist magic-angle trilayer graphene, Science **371**, 1133 (2021).
[112] C. Shen, P. J. Ledwith, K. Watanabe, T. Taniguchi, E. Khalaf, A. Vishwanath, and D. K. Efetov, Dirac spectroscopy of strongly correlated phases in twisted trilayer graphene, Nat. Mater. **22**, 316 (2023).
[113] X. Liu, N. J. Zhang, K. Watanabe, T. Taniguchi, and J. I. A. Li, Isospin order in superconducting magic-angle twisted trilayer graphene, Nat. Phys. **18**, 522 (2022).
[114] H. Kim, Y. Choi, C. Lewandowski, A. Thomson, Y. Zhang, R. Polski, K. Watanabe, T. Taniguchi, J. Alicea, and S. Nadj-Perge, Evidence for unconventional superconductivity in twisted trilayer graphene, Nature (London) **606**, 494 (2022).
[115] S. Turkel, J. Swann, Z. Zhu, M. Christos, K. Watanabe, T. Taniguchi, S. Sachdev, M. S. Scheurer, E. Kaxiras, C. R. Dean, and A. N. Pasupathy, Orderly disorder in magic-angle twisted trilayer graphene, Science **376**, 193 (2022).
[116] H. Zhou, L. Holleis, Y. Saito, L. Cohen, W. Huynh, C. L. Patterson, F. Yang, T. Taniguchi, K. Watanabe, and A. F. Young, Isospin magnetism and spin-polarized superconductivity in Bernal bilayer graphene, Science **375**, 774 (2022).
[117] A. M. Seiler, F. R. Geisenhof, F. Winterer, K. Watanabe, T. Taniguchi, T. Xu, F. Zhang, and R. T. Weitz, Quantum cascade of correlated phases in trigonally warped bilayer graphene, Nature (London) **608**, 298 (2022).
[118] S. C. de la Barrera, S. Aronson, Z. Zheng, K. Watanabe, T. Taniguchi, Q. Ma, P. Jarillo-Herrero, and R. Ashoori, Cascade of isospin phase transitions in Bernal-stacked bilayer graphene at zero magnetic field, Nat. Phys. **18**, 771 (2022).
[119] Y. Zhang, R. Polski, A. Thomson, É. Lantagne-Hurtubise, C. Lewandowski, H. Zhou, K. Watanabe, T. Taniguchi, J. Alicea, and S. Nadj-Perge, Enhanced superconductivity in spin–orbit

proximitized bilayer graphene, Nature (London) **613**, 268 (2023).

[120] L. Holleis, C. L. Patterson, Y. Zhang, H. M. Yoo, H. Zhou, T. Taniguchi, K. Watanabe, S. Nadj-Perge, and A. F. Young, Ising superconductivity and nematicity in Bernal bilayer graphene with strong spin orbit coupling, arXiv:2303.00742.

[121] H. Zhou, T. Xie, A. Ghazaryan, T. Holder, J. R. Ehrets, E. M. Spanton, T. Taniguchi, K. Watanabe, E. Berg, M. Serbyn, and A. F. Young, Half- and quarter-metals in rhombohedral trilayer graphene, Nature (London) **598**, 429 (2021).

[122] H. Zhou, T. Xie, T. Taniguchi, K. Watanabe, and A. F. Young, Superconductivity in rhombohedral trilayer graphene, Nature (London) **598**, 434 (2021).

[123] Y. W. Choi and H. J. Choi, Dichotomy of electron-phonon coupling in graphene moiré flat bands, Phys. Rev. Lett. **127**, 167001 (2021).

[124] M. Koshino and Y.-W. Son, Moiré phonons in twisted bilayer graphene, Phys. Rev. B **100**, 075416 (2019).

[125] H. Ochoa, Moiré-pattern fluctuations and electron-phason coupling in twisted bilayer graphene, Phys. Rev. B **100**, 155426 (2019).

[126] M. Koshino and N. N. T. Nam, Effective continuum model for relaxed twisted bilayer graphene and moiré electron-phonon interaction, Phys. Rev. B **101**, 195425 (2020).

[127] M. Angeli and M. Fabrizio, Jahn–Teller coupling to moiré phonons in the continuum model formalism for small-angle twisted bilayer graphene, Eur. Phys. J. Plus **135**, 630 (2020).

[128] H. Ochoa and R. M. Fernandes, Degradation of phonons in disordered moiré superlattices, Phys. Rev. Lett. **128**, 065901 (2022).

[129] Q. Gao and E. Khalaf, Symmetry origin of lattice vibration modes in twisted multilayer graphene: Phasons versus moiré phonons, Phys. Rev. B **106**, 075420 (2022).

[130] X. Liu, R. Peng, Z. Sun, and J. Liu, Moiré phonons in magic-angle twisted bilayer graphene, Nano Lett. **22**, 7791 (2022).

[131] J. Z. Lu, Z. Zhu, M. Angeli, D. T. Larson, and E. Kaxiras, Low-energy moiré phonons in twisted bilayer van der Waals heterostructures, Phys. Rev. B **106**, 144305 (2022).

[132] W. Miao, C. Li, X. Han, D. Pan, and X. Dai, Truncated atomic plane wave method for subband structure calculations of moiré systems, Phys. Rev. B **107**, 125112 (2023).

[133] E. Cappelluti, J. A. Silva-Guillén, H. Rostami, and F. Guinea, Flat-band optical phonons in twisted bilayer graphene, Phys. Rev. B **108**, 125401 (2023).

[134] S. Carr, S. Fang, Z. Zhu, and E. Kaxiras, Exact continuum model for low-energy electronic states of twisted bilayer graphene, Phys. Rev. Res. **1**, 013001 (2019).

[135] O. Vafek and J. Kang, Continuum effective Hamiltonian for graphene bilayers for an arbitrary smooth lattice deformation from microscopic theories, Phys. Rev. B **107**, 075123 (2023).

[136] J. Kang and O. Vafek, Pseudomagnetic fields, particle-hole asymmetry, and microscopic effective continuum Hamiltonians of twisted bilayer graphene, Phys. Rev. B **107**, 075408 (2023).

[137] Z.-D. Song and B. A. Bernevig, Magic-angle twisted bilayer graphene as a topological heavy fermion problem, Phys. Rev. Lett. **129**, 047601 (2022).

[138] D. Călugăru, M. Borovkov, L. L. H. Lau, P. Coleman, Z.-D. Song, and B. A. Bernevig, Twisted bilayer graphene as topological heavy fermion: II. Analytical approximations of the model parameters, Fiz. Nizk. Temp. **49**, 640 (2023).

[139] J. Yu, M. Xie, B. A. Bernevig, and S. D. Sarma, Magic-angle twisted symmetric trilayer graphene as topological heavy fermion problem, Phys. Rev. B **108**, 035129 (2023).